^{18}F-FDG PET/CT radiomics model from non-small cell lung cancer for preoperative prediction of lymph node metastasis based on overall data and the subset of occult lymph nodes

Ruihe Lai[1] **MD,**
Yuzhi Geng[2] **Msc,**
Dandan Sheng[2] **BSc,**
Chongyang Ding[3] **MD,**
Chunjun Qian[4] **MD,**
Chong Jiang[5] **MD,**
Zhengyang Zhou[6] **MD**

1. Department of Nuclear Medicine, Nanjing Drum Tower Hospital, Clinical College of Nanjing Medical University, Nanjing, China
2. Department of Nuclear Medicine, The Second Affiliated Hospital of Nanjing Medical University, Nanjing, China
3. Department of Nuclear Medicine, The First Affiliated Hospital of Nanjing Medical University, Nanjing, China
4. Hertfordshire College, Changzhou Institute of Technology, Changzhou , China
5. Department of Nuclear Medicine, West China Hospital, Sichuan University, Chengdu, China
6. Department of Radiology, Nanjing Drum Tower Hospital, Clinical College of Nanjing Medical University, Nanjing, China

Keywords: ^{18}F-FDG PET/CT - Non-small cell lung cancer - Radiomics - Occult lymph node metastasis

Corresponding author:
Zhengyang Zhou
Department of Radiology, Nanjing Drum Tower Hospital, Clinical College of Nanjing Medical University, Nanjing, China
zyzhou@nju.edu.cn
Chong Jiang
Department of Nuclear Medicine, West China Hospital, Sichuan University, Chengdu, China
jiangc_nju@163.com,
Chunjun Qian
Hertfordshire College, Changzhou Institute of Technology, Changzhou, China
qiancj@czust.edu.cn

Received:
8 April 2025
Accepted revised:
27 August 2025

Abstract

Objective: Lymph node (LN) staging in lung cancer is crucial for treatment decisions. To develop and validate a positron emission tomography/computed tomography (PET/CT) radiomics model for preoperative estimation of LN metastasis in non-small cell lung cancer (NSCLC). **Subjects and Methods:** A retrospective analysis of 252 NSCLC patients with 548 pathologically confirmed LN, including 227 occult LN, was performed. Clinical and PET/CT features were collected. Eight machine learning models were used for feature selection and radiomics signature (R-signature) construction. Models were developed for both the overall and occult LN groups. Model performance was evaluated using area under the curve (AUC), calibration, and decision curve analysis. **Results:** The random forest-enhanced logistic regression (RFELR) model, based on 20 features, showed the best performance in predicting LN metastasis in both groups. The combined model demonstrated the highest predictive efficacy, with AUC of 0.94 (overall LN) and 0.89 (occult LN) in the training cohort, and 0.95 (overall LN) and 0.78 (occult LN) in the validation cohort. The combined model outperformed clinical, CT, and PET models ($P<0.05$) in both cohorts. Decision curve analysis showed a greater net benefit across a wider range of threshold probabilities for LN metastasis prediction. **Conclusion:** The combined model, integrating clinical, conventional PET/CT, and radiomics features, significantly enhances LN metastasis diagnosis. It shows promise in predicting occult LN metastasis and offers valuable support for personalized therapeutic decisions in NSCLC patients.

Hell J Nucl Med 2025; 28(3): 200-211 *Epub ahead of print: 15 December 2025* *Published online: 30 December 2025*

Introduction

Lung cancer is the second most common cancer and the leading cause of cancer death. Non-small cell lung cancer (NSCLC) the most common subtype of lung cancer, accounts for approximately 85% of all cases [1, 2]. In the context of NSCLC, accurate lymph node (LN) staging holds paramount importance, as it informs various treatment options for patients with NSCLC. Furthermore, there is an increased incidence of occult LN metastasis in early-stage NSCLC [3, 4], which can lead to changes in pathological staging, alterations in therapeutic strategies, and increased psychological stress for patients. Presently, the gold standard methods for preoperative diagnosing LN metastasis involve mediastinoscopy and endobronchial ultrasound-guided transbronchial needle aspiration (EBUS-TBNA). However, these methods cannot be routinely applied to the entire population due to complications, technical constraints, and the physical condition of the patients.

Fluorine-18-fluorodeoxyglucose (^{18}F-FDG) positron emission tomography/computed tomography (PET/CT) proves to be a promising tool for diagnosing LN metastasis in NSCLC when interpreted using volume-based PET parameters, such as baseline total metabolic tumor volume (MTV) and total lesion glycolysis (TLG) [5, 6]. Additionally, guidelines underscore the pivotal role of PET/CT in diagnosing LN metastasis, especially when compared to EBUS-TBNA and mediastinoscopy [7]. While PET/CT conventional parameters have shown improved performance in LN staging, with an estimated sensitivity of 77% and specificity of 86% when compared to CT alone (55% and 81%, respectively) [8, 9], there are still deficiencies in the diagnosis of occult LN metastasis. Occult lymph node metastasis refers to the situation where no suspicious lesions are detected in the hilar and mediastinal LN on PET/CT scans, but postoperative pathological results confirm the presence of lymph node metastasis. The incidence of occult LN metastasis in PET/CT is estimated to be between 15% and 18% [10-12]. Therefore, there is an urgent need for new methods to

improve the detection rate of LN metastasis, especially occult LN metastasis.

Radiomics has emerged as a promising noninvasive technique for characterizing tumor heterogeneity, which aids in assessing therapeutic response, predicting prognosis, and classifying histopathological types in lung cancer [13, 14]. Recent years have witnessed significant progress in applying radiomics for evaluating LN staging in NSCLC [15, 16]. However, there is a paucity of studies concerning the prediction of LN staging using PET/CT LN radiomics for NSCLC. Furthermore, limited research has explored the potential of PET/CT radiomics features for predicting occult LN metastasis. To address these gaps, a retrospective study was conducted to evaluate the effectiveness of PET/CT radiomics in assessing the risk of LN metastasis in NSCLC patients. Additionally, the study examined the potential of a combined model to predict occult LN metastasis, which could have significant implications for clinical treatment decision-making.

Subjects and Methods

Patient data collection

This study was approved by the Ethics Committee of our hospital (Approval No. 2022-255-03). Informed consent from patients was waived. The inclusion criteria were as follows: (I) Patients examined on PET/CT scanners with histologically confirmed NSCLC between January 2017 and November 2023; (II) Patients who underwent ^{18}F-FDG PET/CT imaging with an interval of less than four weeks between imaging and pathological diagnosis. The exclusion criteria were as follows: (I) Without lymphadenectomy or LN biopsy pathology. (II) Patients who had undergone prior radiotherapy or chemotherapy before PET/CT imaging; (III) Medical data incomplete; (IV) patients with a history of other malignant tumors.

In total, 252 patients were included in this study. The patients who satisfied the inclusion criteria were identified for the whole patient cohort, which is also referred to as the overall LN group (n=252). Additionally, patients with clinical stage N0M0 LN and having a short diameter (SD) ≤10mm and SUVmax ≤2.5 were selected from the whole patient cohort to form the occult LNs group (n=137). The patients enrolled flowchart is shown in Figure 1A. In overall LN group, there were 167 patients with N0 stage, 19 patients with N1 stage, 53 patients with N2 stage, and 13 patients with N3 stage, while in occult LN group, there were 118 patients with N0 stage, 6 patients with N1 stage, 13 patients with N2 stage. Then, these patients were divided into the LN(+) group and LN(–) group based on pathological reports. The LN enrolled flowchart is shown in Figure 1B. The inclusion criteria were as follows: (I) According to the pathology report defined with the N staging standard of the eighth edition (17) to locate and select surgical or supraclavicular biopsy LN station; (II) 1-2 LN per station were selected with the maximum SUVmax; (III) The number of LN selected in each LN station was limited by the number of actual positive or negative pathological results. The exclusion criteria were as follows: the negative LN stations of LN(+) patients were excluded to ensure as much as possible the LN selected are truly pathologically positive (16).

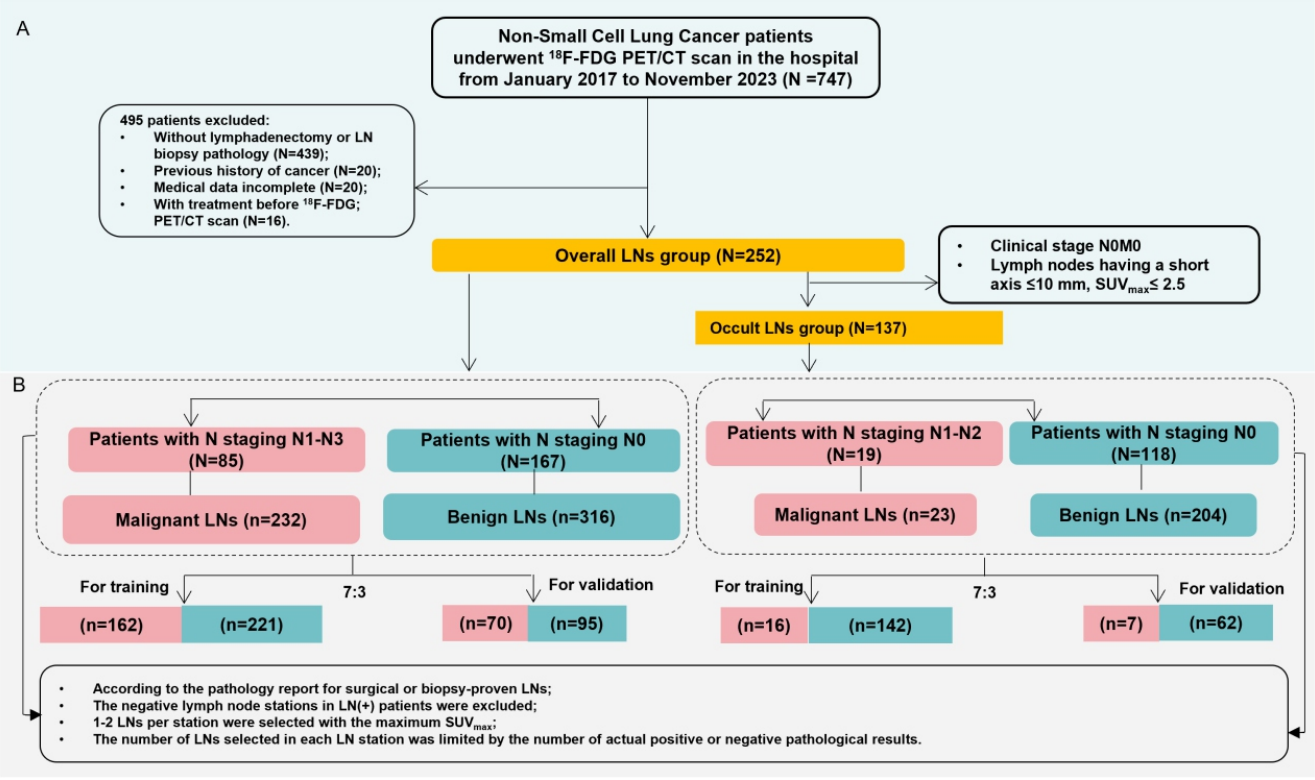

Figure 1. Flow diagram of the selection of patients (A) and LN (B).

^{18}F-FDG PET/CT imaging

All patients were instructed to fast for a minimum of six hours prior to the examination, avoiding the intake of sugary fluids or glucose, whether orally or intravenously, and ensuring that their fasting blood glucose level remained within the range of ≤10.0mmol/L. Prior to tracer administration, each patient's weight was measured to calculate the standardized uptake value. A dose of 3.70MBq/kg of ^{18}F-FDG was administered intravenously, and imaging acquisition began 60 minutes after the tracer injection, covering the region from the base of the skull to the upper thighs. Each bed position was scanned for two minutes. Computed tomography acquisition data were used for attenuation correction, and the corrected PET images were reconstructed using ordered subset expectation maximization with a matrix size of 144×144. The PET and CT images volume of interest drawing and radiomics processing then registered and fused using Syntegra software.

Volume of interest drawing and radiomics processing

The PET/CT images were transferred to 3D Slicer software (version 4.8.0; available at: http://www.slicer.org). Two physicians, RH.L with fourteen experience in thoracic PET/CT tumor diagnosis and YZ.G with ten years of experience in the same field, delineated the LN. For CT image delineation, a manual polygonal region of interest (ROI) was sketched along the edges of the lesions, with care taken to exclude adjacent normal tissue as much as possible. In the case of PET image delineation, the 3D Slicer software employed a semi-automatic region-growing algorithm to generate the VOI. In cases of discrepancies, a senior nuclear medicine expert re-evaluated and reviewed the VOI. Prior to feature extraction, the PET images underwent preprocessing, including resampling to 1×1×1mm^3 voxel size using bilinear interpolation, and discretization to 128 fixed gray levels [18]. Following the manual segmentation, Pyradiomics package (accessible at http://www.radiomics.io/Pyradiomics.html), an open-source resource, were utilized to extract various features. This process yielded 1967 features for both PET and CT (Table 1).

In addition to radiomics features, PET/CT conventional features were also collected, which included both CT morphological parameters and PET metabolic parameters. The CT morphological parameters encompassed lesion location, long diameter (LD), SD, LD/SD, CTave, presence of calcification. Positron emission tomography metabolic parameters, on the other hand, included SUVmax, MTV and TLG. We measured these parameters using dedicated software (CompassView 5.0, Philips). To calculate MTV, a circular ROI was drawn to encompass the entire lesion, while excluding other high metabolic lesions, using a threshold of 41% [19] SUVmax as the boundary. Metabolic tumor volume was automatically generated by the system. Total lesion glycolysis was then calculated as the product of SUVmean and MTV (TLG=SUVmean × MTV).

Radiomics feature selection and signature construction

A total of 3934 features from LN were extracted using the radiomics library in Python, including 1967 CT features and 1967 PET features (Table 1). The extracted features contain the original, LoG, Wavelet, Square, SquareRoot, Logarithm, Exponential, Gradient and LBP3D features with different parameter setting. To minimize subjective differences with different VOI segmentation methods, the intraclass correlation coefficients (ICC) for radiomics feature analysis and selection were set at 0.8 [20]. To be noted that the model in ICC analysis was "single random raters". Subsequently, to avoid overfitting, feature selection based on the conventional machine learning method was performed. For feature selection and R-signature constrtuction, we employed eight classical

Table 1. *Classification of extracted features for both PET and CT.*

	Shape	First-order	GLCM	GLRLM	GLSZM	GLDM	NGTDM	Total
Original	14	18	24	16	16	14	5	107
Log-sigma	-	72	96	64	64	56	20	372
Wavelet	-	144	192	128	128	112	40	744
Square	-	18	24	16	16	14	5	93
Squareroot	-	18	24	16	16	14	5	93
Logarithm	-	18	24	16	16	14	5	93
Exponential	-	18	24	16	16	14	5	93
Gradient	-	18	24	16	16	14	5	93
LBP3D	-	54	72	48	48	42	15	279
Total	14	378	504	336	336	294	105	1967

methods: extreme gradient boosting (XGBoost), random forest classifier (RFC), logistic regression (LR), least absolute shrinkage and selection operator (LASSO), gradient boosting decision tree (GBC), logistic regression + recursive feature elimination (RFELR), extreme gradient boosting (XGB), and linear discriminant analysis (LDA). The penalty parameters in these methods were optimized using ten-fold cross-validation. Feature selection models were used to identify the top 20 features with the highest weights and the R-signature was constructed based on the selected features. Finally, optimal candidate R-signature was selected to construct model. The R-signature in the overall LN group is designated as R-signature 1, while the R-signature in the occult LNs group is designated as R-signature 2.

Table 2. *The top 20 features for construction of R-signature for both overall LN group and occult LN group.*

Overall LNs group	Occult LNs group
wavelet-LHL_glcm_ClusterShade	original_firstorder_Interquartil
wavelet-LHL_ngtdm_Contrast	log-sigma-3-mm-3D_firstorder_Mea
lbp-3D-m1_firstorder_Variance	log-sigma-3-mm-3D_firstorder_Rob
original_shape_SurfaceVolumeRati	log-sigma-3-mm-3D_firstorder_Var
original_glrlm_RunPercentage	log-sigma-3-mm-3D_glcm_ClusterPr
log-sigma-3-mm-3D_firstorder_Ske	log-sigma-5-mm-3D_firstorder_Kur
log-sigma-5-mm-3D_glrlm_LongRunL	log-sigma-5-mm-3D_firstorder_Rob
log-sigma-7-mm-3D_glrlm_LongRunL	log-sigma-7-mm-3D_glcm_JointEntr
log-sigma-9-mm-3D_glcm_ClusterPr	log-sigma-7-mm-3D_glcm_SumEntrop
log-sigma-9-mm-3D_gldm_LargeDepe	wavelet-HLL_glcm_ClusterShade
wavelet-LLH_glrlm_LongRunEmphasi	gradient_firstorder_Median
wavelet-LHL_glrlm_RunPercentage	original_glrlm_LongRunHighGrayLe
wavelet-LHH_glrlm_RunVariance	log-sigma-9-mm-3D_glcm_Autocorre
wavelet-HLL_glrlm_RunPercentage	log-sigma-9-mm-3D_glcm_JointAver
wavelet-HLL_glrlm_ShortRunLowGra	log-sigma-9-mm-3D_glcm_SumAverag
square_glrlm_RunLengthNonUniform	log-sigma-9-mm-3D_gldm_LargeDepe
squareroot_firstorder_Mean	wavelet-HLH_firstorder_Kurtosis
squareroot_firstorder_RootMeanSq	wavelet-LLL_glrlm_LongRunHighGra
logarithm_firstorder_Mean	squareroot_glrlm_LongRunHighGray
logarithm_firstorder_RootMeanSqu	logarithm_glrlm_LongRunHighGrayL

(Continued)

Statistical analysis

All statistical analyses were conducted using SPSS 22.0 software (IBM Corporation) and Medcalc statistical software (version 20.0.22). Categorical variables were analyzed by Pearson's chi-square test (or Fisher's exact test when necessary), continuous variables were compared by Student t-test or Mann-Whitney U test. The optimal threshold (cut-off point) was determined by maximizing the Youden index (sensitivity + specificity - 1) through receiver operating characteristic (ROC) curve analysis. To assess the clinical data differences between the training and validation cohorts, Pearson's chi-square test (or Fisher's exact test when necessary) was used for categorical variables, and the Mann-Whitney U test was used for comparing quantitative parameters. The optimal threshold (cut-off point) was determined by maximizing the Youden index (sensitivity + specificity - 1) through ROC curve analysis. Univariate and multivariate logistic regression analysis was performed to identify the independent predictive factors for model establishment. The discriminative ability of the models was evaluated using the AUC operating characteristic curve and the Delong test was used to compare AUC between groups. To evaluate calibration performance, calibration curves were generated for all cohorts. The clinical usefulness of the radiomics nomogram was evaluated using decision curve analysis (DCA). A P-value less than 0.05 was considered statistically significant.

Results

Clinical characteristics

A total of 548 LN and 227 occult LNs from 252 patients were identified in the present study and were further assigned to either the training cohort or validation cohort. Of the 548 LNs, and 70% (n=383) were assigned to the training cohort by stratified sampling; 162 LN were malignant, and 221 were benign. The remaining 30% (n=165) were selected for the validation cohort; 70 were malignant and 95 were benign. Of the 227 occult LN, and 70% (n=158) were assigned to the training cohort by stratified sampling; 16 LN were malignant,

and 142 were benign. The remaining 30% (n=69) were selected for the validation cohort; 7 were malignant and 62 were benign.

There was no statistically significant difference in the clinical characteristics between the training cohorts and the validation cohort in both overall LN group and occult LN group as shown in Table 3.

Radiomics feature selection and signature construction

A total of 2,659 features with an ICC greater than 0.8 were retained. Among the eight traditional machine models, RFELR yielded the best performance. Subsequently, the top 20 features were selected. In overall LN group, the selected features included 2 original, 5 LoG, 7 Wavelet, 1 Square, 2 SquareRoot, 2 Logarithm, and 1 LBP3D features (Table 2). While in occult LN group, the selected features consisted of 2 original, 12 LoG, 3 Wavelet, 1 SquareRoot, 1 Logarithm, and 1 Gradient feature (Table 2). The top 20 features were selected to construct the R-signature using RFELR for the two groups.

The optimal cut-off values for were determined to be 0.487 and 0.137 for R-signature1 and R-signature2, separately. The AUC values of R-signature were 0.92 and 0.89 in the training and validation cohort of overall LN group, while in occult LN group, the AUC were 0.86 and 0.67, respectively.

Univariate and multivariate logistic regression in the training cohort

In univariate logistic regression analysis, parameters like age, gender, pathological type, location, LD, SD, LD/SD, CTave, calcification, SUVmax, MTV, and TLG in overall LN group and gender, location, SD, LD/SD, SUVmax, MTV, and TLG in occult LN group exhibited a significant association with LN metastasis (all $P<0.05$). In the multivariable logistic regression analysis, pathological type (OR=0.465, P=0.007), location (OR=0.299, P=0.005), LD (OR=2.724, P=0.026), calcification (OR=22.147, P=0.001), and SUVmax (OR=7.968, $P<0.001$) in overall LN group and gender (OR=12.880, $P<0.001$), location (OR=0.128, P=0.014), LD/SD (OR=0.236, P=0.030), and SUVmax (OR=6.844, P=0.027) in occult LN group were identified as independent factors for predicting LN metastasis (Table 4).

Model construction

The R-signature, along with the significant parameters from the above multifactorial analysis, was used to construct the model. Then, five models were established for overall LN group: The clinical model (pathological type), the CT model (location, LD, calcification), the PET model (SUVmax), the Radiomics model (R-signature1) and the combined model (pathological type, location, LD, calcification, SUVmax, R-signature1), another five models were established for occult LN group: The clinical model (gender), the CT model (location, LD/SD), the PET model (SUVmax), the Radiomics model (R-signature2) and the combined model (gender, location, LD/SD, SUVmax, R-signature2) (Table 5).

Evaluate and validate the performance of the model

The AUC values, sensitivity (SEN), and specificity (SPE) for these models in the training cohort were as follows: Clinical model - 0.57, 0.85, 0.29, CT model - 0.82, 0.67, 0.85, PET model - 0.90, 0.81, 0.84, Radiomics model - 0.92, 0.78, 0.91, and Combined model - 0.94, 0.82, 0.90 in overall LN group and Clinical model - 0.76, 0.71, 0.88, CT model - 0.67, 0.70, 0.61, PET model - 0.77, 0.88, 0.71, Radiomics model - 0.89, 0.81, 0.87 ,and Combined model - 0.95, 1.00, 0.78 in occult LN group (Figure 2 A, B). In the validation cohort, the AUC values, SEN, and SPE were: Clinical model - 0.58, 0.87, 0.27, CT model - 0.67, 0.70, 0.61, PET model - 0.80, 0.77, 0.80, Radiomics model - 0.86, 0.71, 0.88, and Combined model - 0.89, 0.74, 0.89 in overall LN group and Clinical model - 0.61, 0.86, 0.36, CT model - 0.66, 0.43, 0.95, PET model - 0.58, 0.71, 0.45, Radiomics model - 0.867, 0.86, 0.53, and Combined model - 0.78, 0.86, 0.65 in occult LN group (Figure 2 C, D).

Among these five models, the combined model displayed the highest predictive effectiveness (Figure 2). Compared to the clinical model, CT model and PET model, the AUC of the combined model exhibits a statistically significant difference in both the training ($Z=16.77$, $P<0.001$; $Z=6.33$, $P<0.001$, $Z=4.05$, $P<0.001$ in overall LN group and $Z=3.87$, $P<0.001$; $Z=3.06$, $P=0.002$, $Z=2.59$, $P=0.001$ in occult LN group) and validation cohort ($Z=8.26$, $P<0.001$; $Z=4.62$, $P<0.001$, $Z=4.15$, $P<0.001$ in overall LN group). While the AUC of the combined model is statistically significantly different only when compared to the clinical model in the validation cohort of occult LN group ($Z=2.60$, $P=0.009$).

Calibration curves showed good agreement between the actual and predicted probabilities of occurrence for the combined model in both the training and validation cohorts and the performance of the combined model was visualized using a nomogram (Figure 3). Finally, The DCA plot clearly illustrates that the combined model outperformed the others by achieving the highest net benefit over a wider range of reasonable threshold probabilities (Figure 4).

Discussion

Lymph node metastasis has been confirmed as an important prognostic factor in NSCLC and plays a critical role in guiding treatment decisions [21, 22]. Therefore, lymph node staging is a crucial step in the early detection of lung cancer. The current study managed to develop a PET/CT radiomics model. The proposed combined model achieved AUC of 0.94, 0.95 for LN metastasis prediction, and 0.892, 0.78 for occult LN prediction, in the training and validation cohort, respectively.

The identification of LN metastasis in lung cancer relies on clinical and imaging features such as gender, tumor size, location, histopathology, and SUVmax [23-25]. This study also found that adenocarcinoma histology, hilum-located lymph nodes, LD >7.8mm, and SUVmax >3.56 are associated with LN metastasis, while female gender, LD /SD ≤1.53, hilum-located nodes, and SUVmax >1.78 are linked to occult LN metastasis. However, models based on clinical, PET, and CT features in validation cohort only achieved an AUC of 0.67 to 0.77 for LN metastasis prediction, and 0.58-0.66 for occult LN metastasis prediction, which were far from meeting clinical

Table 3. *Demographic, clinical and PET/CT characteristics in training and validation cohorts for overall LN group and occult LN group.*

Characteristics	Overall LN group				Occult LN group			
	Overall (n=548)	Training (n=383)	Validation (n=165)	P value	Overall (n=227)	Training (n=158)	Validation (n=69)	P value
Age (years), ≤60/＞60	161/387	109/274	52/113	0.471	78/149	60/98	18/51	0.083
Gender, male/female	333/215	233/150	100/65	0.960	140/87	94/64	46/23	0.307
Smoke, no/ yes	379/169	260/123	119/46	0.325	158/69	110/48	48/21	0.993
Alcohol consumption, no/ yes	458/90	321/62	137/28	0.821	189/38	130/28	59/10	0.549
Pathological type, adenocarcinoma /squamous carcinoma	422/126	295/88	127/38	0.989	173/54	119/39	54/15	0.632
Location (region), hilar / mediastinal	81/467	51/332	30/135	0.141	18/209	12/146	6/63	0.778
Long diameter(mm), mean±SD	13.06±5.09	13.12±4.99	12.90±5.35	0.644	10.53±2.70	10.35±2.66	10.94±2.78	0.132
Short diameter(mm), mean±SD	8.15±3.54	8.12±3.47	8.23±3.73	0.739	6.07±1.47	5.97±1.35	6.28±1.71	0.157
LD/SD, mean±SD	1.69±0.55	1.71±0.58	1.65±0.48	0.203	1.80±0.56	1.78±0.50	1.85±0.67	0.445
CTave(HU), mean±SD	33.75±22.34	32.91±21.96	35.72±23.17	0.177	27.83±24.35	27.22±23.42	29.22±26.46	0.571
Calcification, no/ yes	28/520	19/364	9/156	0.810	11/216	5/153	6/63	0.094
SUVmax, mean±SD	4.71±4.48	4.67±4.36	4.82±4.75	0.709	1.68±0.46	1.68±0.46	1.69±0.47	0.842
MTV(cm^3), mean±SD	2.09±2.35	2.13±2.38	2.00±2.31	0.555	0.74±0.88	0.70±0.94	0.84±0.72	0.292
TLG, mean±SD	9.29±19.13	8.82±15.57	10.38±25.57	0.381	1.03±1.14	0.98±1.18	1.14±1.07	0.313
R-signature（rfelr）, mean±SD	0.44±0.28	0.43±0.27	0.47±0.29	0.072	0.11±0.04	0.11±0.04	0.11±0.04	0.411

LN, lymph node; LD, Long diameter; SD, Short diameter; SUVmax, maximum standardized uptake value; MTV, metabolic tumor volume; TLG, total lesion glycolysis; categorical variables were analyzed by Pearson χ2 test and Fisher exact test, continuous variables were compared by Student t-test and Mann-Whitney U test.

Table 4. *Logistic analyses of overall LN group and occult LN group for patients in the training cohort.*

Characteristics	Overall LN group (n=548)				Characteristics	Occult LN group (n=227)			
	Univariable		Multivariable			Univariable		Multivariable	
	OR (95% CI)	P value	OR (95% CI)	P value		OR (95% CI)	P value	OR (95% CI)	P value
Age (years), ≤60/＞60	1.243 (0.790-1.957)	0.347			Age (years), ≤60/＞60	1.391 (0.458-4.219)	0.560		
Gender, male/female	1.534 (1.013-2.323)	0.043	1.228 (0.788-1.914)	0.365	Gender, male/female	12.880 (2.814-58.954)	＜0.001	12.880 (2.814-58.954)	＜0.001
Smoke, no/ yes	0.705 (0.454-1.096)	0.120			Smoke, no/yes	0.000 (0.000-0.000)	0.997		
Alcohol consumption, no/ yes	0.654 (0.370-1.157)	0.144			Alcohol consumption, no/ yes	0.000 (0.000-0.000)	0.998		
Pathological type, adenocarcinoma /squamous carcinoma	0.427 (0.253-0.719)	0.001	0.465 (0.267-0.809)	0.007	Pathological type, adenocarcinoma /squamous carcinoma	0.000 (0.000-0.000)	0.998		
Location, hilar / mediastinal	3.924 (2.065-7.455)	＜0.001	0.299 (0.128-0.695)	0.005	Location, #10-11/# 1-9	0.114 (0.031-0.419)	0.001	0.128 (0.025-0.655)	0.014
Long diameter r (mm), ≤14.5/＞14.5	7.800 (4.720-12.889)	＜0.001	2.724 (1.129-6.574)	0.026	Long diameter(mm), ≤11.5/＞11.5	1.852 (0.647-5.299)	0.251		
Short diameter (mm), ≤8.5/＞8.5	12.360 (7.421-20.586)	＜0.001	2.002 (0.864-4.638)	0.105	Short diameter(mm), ≤5.5/＞5.5	11.962 (1.538-93.025)	0.018	4.597 (0.502-42.113)	0.177

(Continued)

LD/SD, ≤1.59/＞1.59	0.380 (0.250-0.577)	＜0.001	0.728 (0.333-1.409)	0.409	LD/SD, ≤1.53/＞1.53	0.211 (0.069-0.643)	0.006	0.236 (0.064-0.869)	0.030
CTave(HU), ≤30.90/＞30.90	3.797 (2.402-6.001)	＜0.001	1.111 (0.556-2.220)	0.767	CTave(HU), ≤21.30/＞21.30	3.923 (0.857-17.951)	0.078		
Calcification, yes/ no	6.667 (1.518-29.278)	0.012	22.147 (3.370-145.532)	0.001	Calcification, yes/ no	188 (0.000-0.000)	0.999		
SUVmax, ≤3.56/＞3.56	22.457 (13.184-38.252)	＜0.001	7.968 (3.627-17.502)	＜0.001	SUVmax, ≤1.78/＞1.78	8.778 (1.923-40.059)	0.005	6.844 (1.241-37.751)	0.027
MTV(cm^3), ≤1.57/＞1.57	10.528 (6.537-16.956)	＜0.001	1.396 (0.550-3.543)	0.4834	MTV(cm^3), ≤0.87/＞0.87	4.604 (1.587-13.354)	0.005	0.835 (0.115-6.044)	0.858
TLG, ≤3.37/＞3.37	21.782 (12.631-37.560)	＜0.001	2.483 (0.887-6.948)	0.083	TLG, ≤1.08/＞1.08	5.810 (1.897-17.799)	0.002	2.837 (0.347-23.227)	0.331

LN, lymph node; LD, Long diameter ; SD, Short diameter; SUVmax, maximum standardized uptake value; MTV, metabolic tumor volume; TLG, total lesion glycolysis; OR, odds ratio: ,CI, condence interval;

Table 5. *The variables of predictive models included in this study.*

Models	Overall LN group	Occult LN group
Clinical model	Pathological type	Gender
CT model	Location, LD, Calcification	Location, LD/SD
PET model	SUVmax	SUVmax
Radiomics model	R-signature1	R-signature2
Combined model	Pathological type, Location, LD, Calcification, SUVmax, R-signature	Gender, Location, LD/SD, SUVmax, R-signature

LD, Long diameter; SD, Short diameter; SUVmax, maximum standardized uptake value

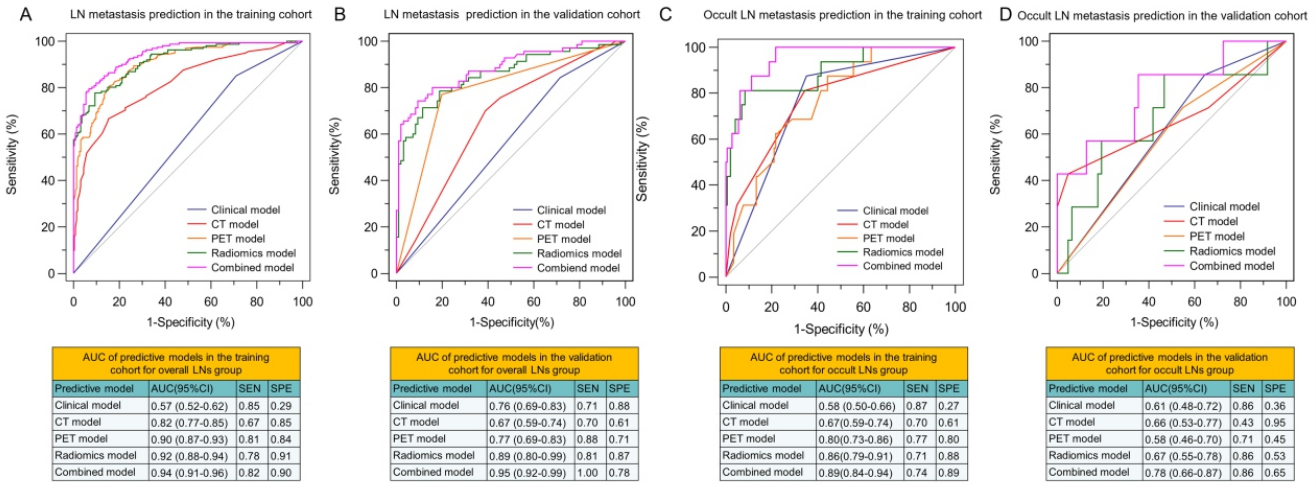

AUC of predictive models in the training cohort for overall LNs group

Predictive model	AUC(95%CI)	SEN	SPE
Clinical model	0.57 (0.52-0.62)	0.85	0.29
CT model	0.82 (0.77-0.85)	0.67	0.85
PET model	0.90 (0.87-0.93)	0.81	0.84
Radiomics model	0.92 (0.88-0.94)	0.78	0.91
Combined model	0.94 (0.91-0.96)	0.82	0.90

AUC of predictive models in the validation cohort for overall LNs group

Predictive model	AUC(95%CI)	SEN	SPE
Clinical model	0.76 (0.69-0.83)	0.71	0.88
CT model	0.67 (0.59-0.74)	0.70	0.61
PET model	0.77 (0.69-0.83)	0.88	0.71
Radiomics model	0.89 (0.80-0.99)	0.81	0.87
Combined model	0.95 (0.92-0.99)	1.00	0.78

AUC of predictive models in the training cohort for occult LNs group

Predictive model	AUC(95%CI)	SEN	SPE
Clinical model	0.58 (0.50-0.66)	0.87	0.27
CT model	0.67(0.59-0.74)	0.70	0.61
PET model	0.80(0.73-0.86)	0.77	0.80
Radiomics model	0.86(0.79-0.91)	0.71	0.88
Combined model	0.89(0.84-0.94)	0.74	0.89

AUC of predictive models in the validation cohort for occult LNs group

Predictive model	AUC(95%CI)	SEN	SPE
Clinical model	0.61 (0.48-0.72)	0.86	0.36
CT model	0.66 (0.53-0.77)	0.43	0.95
PET model	0.58 (0.46-0.70)	0.71	0.45
Radiomics model	0.67 (0.55-0.78)	0.86	0.53
Combined model	0.78 (0.66-0.87)	0.86	0.65

Figure 2. Receiver operating characteristic curves of predictive mode for lymph nodes metastasis in overall LN group and occult LN group. Receiver operating characteristic curves of models to predict lymph nodes metastasis in the training (A) and validation cohort (B). Receiver operating characteristic curves of models to predict occult lymph nodes metastasis in the training (C) and validation cohort (D).

requirements. Therefore, further investigation is needed to identify more valuable radiographic features for predicting LN metastasis, particularly occult LN metastasis, to enhance clinical utility.

Radiomics, which enables the quantitative extraction of high-dimensional radiological features, offers a promising approach for more accurate evaluation of lymph node status in lung cancer. Several studies have been successful in recognizing LN metastasis, which yielded AUC values of 0.78 to 0.92 in the training cohort and 0.73 to 0.91 in the validation cohort [26-29]. However, most studies have primarily focused on extracting features from the primary tumor, with little attention given to the radiomics features of the LN themselves. Xie Y et al. (2021) [16] reporting the use of CT features to predict NSCLC LN metastasis, achieving AUC of 0.85 and 0.83 in the training and validation cohorts, respectively. Moreover, Ouyang et al. (2021) [30] revealed that PET radiomics signature showing good diagnostic efficacy with AUC of 0.79 and 0.82 in the training and validation cohorts, respectively. In this study, we extracted LN imaging features from both PET and CT to develop the R-signature. The AUC was 0.92 in the training cohort and 0.86 in the validation cohort, demonstrating that our model outperforms previous studies.

Several studies [31-34] have shown that radiomics features of primary tumors can predict occult LN metastasis with an AUC ranging from 0.78 to 0.97. Despite such inspiring success, the above radiomics studies were limited in primary tumor information, and the added value of PET radiomics features for occult LN prediction in NSCLC are still ambiguous. The current study demonstrated that the combined model, which integrates clinical parameters, PET/CT conventional features, and R-signature proved capable of predicting occult LN metastasis with the AUC of 0.89 and 0.78 in the training and validation cohorts, respectively, make it superior to single-modal models based on clinical, PET or CT alone for ONM prediction. Although the slightly lower performance in the validation cohort, it still provides valuable insights. We speculate that the lower performance in the validation cohort may be due to class imbalance and the low number of positive samples.

The optimal machine learning model in both groups of this study was random forest-enhanced logistic regression (RFELR), which builds a LR model and removes the weakest

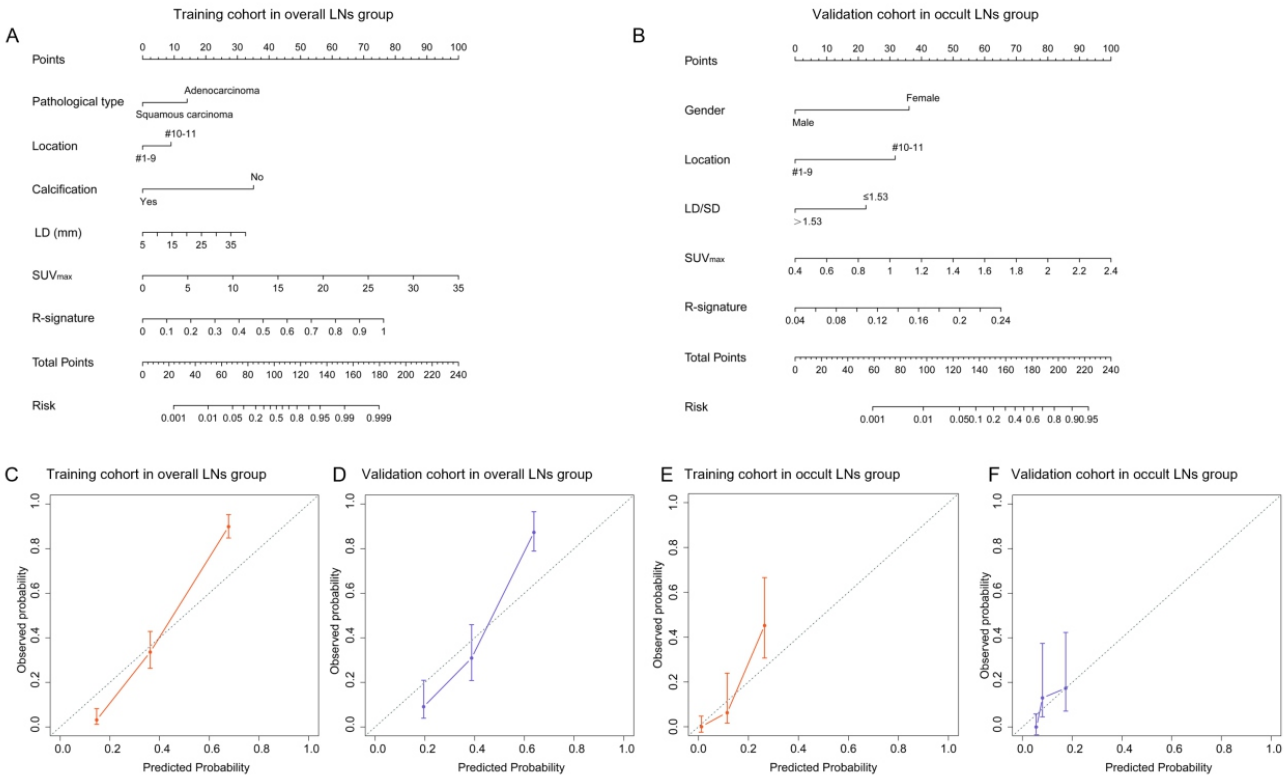

Figure 3. Combined nomogram and calibration curves for predicting LN metastasis. (A) Combined nomogram for overall LN group in the training cohort. (B) Combined nomogram for occult LN group in the training cohort. (D, E) Calibration curve for overall LN group in the training and validation cohorts. (E, F) Calibration curve for occult LN group in the training and validation cohorts.

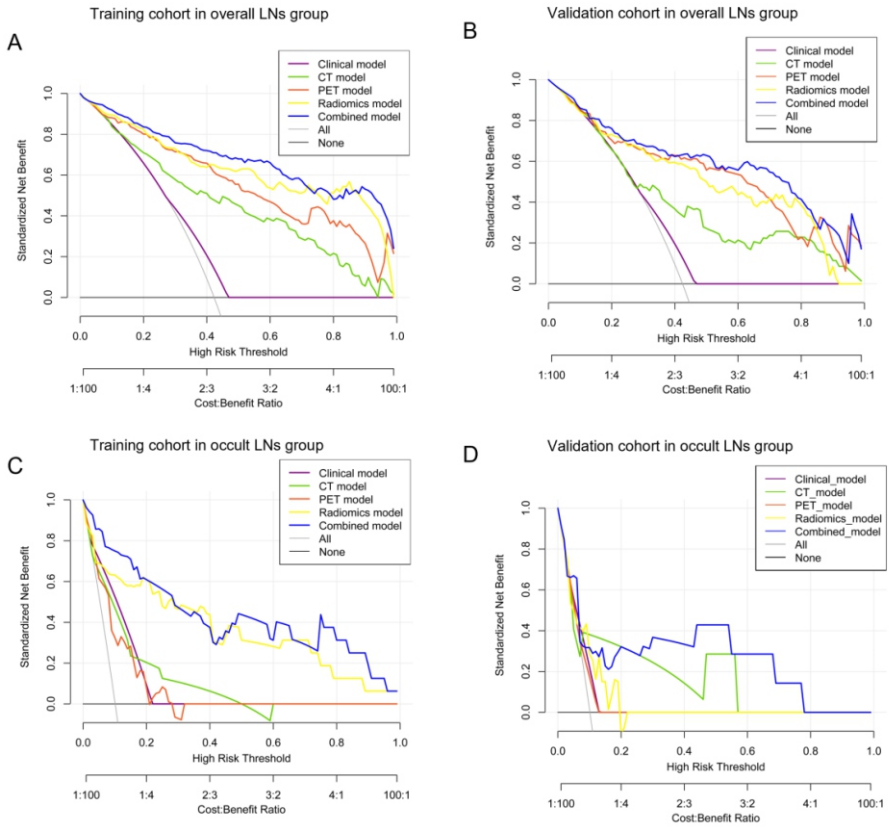

Figure 4. Decision curve analysis of the models for predicting LN metastasis. (A, B) Decision curve analysis for overall LN group in the training and validation cohort. (C, D). Decision curve analysis for occult LN group in the training and validation cohort.

features, repeating this process on the new feature set until the desired number of features is reached. This feature selection method is known as recursive feature elimination (RFE). Random forest-enhanced logistic regression is a classic model known for its stability, particularly with small sample sizes. The RFELR machine learning model is suitable for this study, particularly for the occult LN group, which exhibits a class imbalance, with a considerable disparity between the number of positive and negative cases.

This study still had some limitations. First, as a retrospective study, selection bias was inevitable. Second, although we employed the RFELR machine learning model, which is tailored for small sample sizes, the class imbalance within the occult lymph node group may lead to a model bias, favoring the prediction of the category with a higher sample. Third, although we have tried our best to accurately align the lymph node locations between the PET/CT images and surgical resection or EBUS-TBNA, completely eliminating matching bias remains challenging. Finally, our study did not include clinical information such as tumor markers, a study [35] have shown that these parameters are not independent risk factors for LN metastasis; however, a comprehensive assessment is still required.

In conclusion, radiomics model of LN can serve as predictors for LN metastasis in patients with NSCLC. When PET/CT radiomics features, clinical features, and PET/CT conventional features are integrated into a combined model, it enhances the accuracy of predicting LN metastasis in patients with NSCLC compared to using CT or PET models independently. Furthermore, the combined model is reliable in predicting occult LN for guiding individualized decisions.

Funding

This study was funded by Nanjing Health Science and Technology Development Special Fund (YKK24090).

Bibliography

1. US Preventive Services Task Force, Krist AH, Davidson KW et al. Screening for Lung Cancer: US Preventive Services Task Force Recommendation Statement. *JAMA* 2021; 325: 962-70.
2. Siegel RL, Miller KD, Wagle NS et al. Cancer statistics, 2023. *CA Cancer J Clin* 2023; 73: 17-48.
3. Seto K, Kuroda H, Yoshida T et al. Higher frequency of occult lymph node metastasis in clinical N0 pulmonary adenocarcinoma with ALK rearrangement. *Cancer Manag Res* 2018; 10: 2117-24.
4. Sun J, Wu S, Jin Z et al. Lymph node micrometastasis in non-small cell lung cancer. *Biomed Pharmacother Biomedecine Pharmacother* 2022; 149: 112817.
5. Sun J, Li Y, Gong F et al. The diagnostic value of PET/CT for the lymph node metastasis in Asian patients with non-small cell lung cancer: A meta-analysis. *Hell J Nucl Med* 2022; 25: 196-204.
6. Hua J, Li L, Liu L et al. The diagnostic value of metabolic, morphological and heterogeneous parameters of ^{18}F-FDG PET/CT in mediastinal lymph node metastasis of non-small cell lung cancer. *Nucl Med Commun* 2021; 42: 1247-53.
7. Howington JA, Blum MG, Chang AC et al. Treatment of stage I and II non-small cell lung cancer: Diagnosis and management of lung cancer, 3rd ed: American College of Chest Physicians evidence-based clinical practice guidelines. *Chest* 2013; 143: e278S-e313S.
8. Shim SS, Lee KS, Kim B-T et al. Non-small cell lung cancer: prospective comparison of integrated FDG PET/CT and CT alone for preoperative staging. *Radiology* 2005; 236: 1011-9.
9. Sobic-Saranovic D, Petrusic I, Artiko V et al. Comparison of ^{18}F-FDG PET/CT and MDCT for staging/restaging of non-small cell lung cancer. *Neoplasma* 2015; 62: 295-301.
10. Miao H, Shaolei L, Nan L et al. Occult mediastinal lymph node metastasis in FDG-PET/CT node-negative lung adenocarcinoma patients: Risk factors and histopathological study. *Thorac Cancer* 2019; 10: 1453-60.
11. Li L, Ren S, Zhang Y et al. Risk factors for predicting the occult nodal metastasis in T1-2N0M0 NSCLC patients staged by PET/CT: potential value in the clinic. *Lung Cancer Amst Neth* 2013; 81: 213-7.
12. Park SY, Yoon J-K, Park KJ et al. Prediction of occult lymph node metastasis using volume-based PET parameters in small-sized peripheral non-small cell lung cancer. *Cancer Imaging Off Publ Int Cancer Imaging Soc* 2015; 15: 21.
13. Liu C, Zhao W, Xie J et al. Development and validation of a radiomics-based nomogram for predicting a major pathological response to neoadjuvant immunochemotherapy for patients with potentially resectable non-small cell lung cancer. *Front Immunol* 2023; 14: 1115291.
14. Sun J, Li F, Yang J et al. Pretherapy investigations using highly robust visualized biomarkers from CT imaging by multiple machine-learning techniques toward its prognosis prediction for ALK-inhibitor therapy in NSCLC: a feasibility study. *J Cancer Res Clin Oncol* 2023; 149: 7341-53.
15. Zhong Y, She Y, Deng J et al. Deep Learning for Prediction of N2 Metastasis and Survival for Clinical Stage I Non-Small Cell Lung Cancer. *Radiology* 2022; 302: 200-11.
16. Xie Y, Zhao H, Guo Y et al. A PET/CT nomogram incorporating SUVmax and CT radiomics for preoperative nodal staging in non-small cell lung cancer. *Eur Radiol* 2021; 31: 6030-8.
17. Asamura H, Chansky K, Crowley J et al. The International Association for the Study of Lung Cancer Lung Cancer Staging Project: Proposals for the Revision of the N Descriptors in the Forthcoming 8th Edition of the TNM Classification for Lung Cancer. *J Thorac Oncol Off Publ Int Assoc Study Lung Cancer* 2015; 10: 1675-84.
18. Tixier F, Le Rest CC, Hatt M et al. Intratumor heterogeneity characterized by textural features on baseline ^{18}F-FDG PET images predicts response to concomitant radiochemotherapy in esophageal cancer. *J Nucl Med Off Publ Soc Nucl Med* 2011; 52: 369-78.
19. Meignan M, Sasanelli M, Casasnovas RO et al. Metabolic tumour volumes measured at staging in lymphoma: methodological evaluation on phantom experiments and patients. *Eur J Nucl Med Mol Imaging* 2014; 41: 1113-22.
20. Shrout PE, Fleiss JL. Intraclass correlations: uses in assessing rater reliability. *Psychol Bull* 1979; 86: 420-8.
21. Postmus PE, Kerr KM, Oudkerk M et al. Early and locally advanced non-small-cell lung cancer (NSCLC): ESMO Clinical Practice Guidelines for diagnosis, treatment and follow-up. *Ann Oncol Off J Eur Soc Med Oncol* 2017; 28: iv1-iv21.
22. Nicholson AG, Chansky K, Crowley J et al. The International Association for the Study of Lung Cancer Lung Cancer Staging Project: Proposals for the Revision of the Clinical and Pathologic Staging of Small Cell Lung Cancer in the Forthcoming Eighth Edition of the TNM Classification for Lung Cancer. *J Thorac Oncol Off Publ Int Assoc Study Lung Cancer* 2016; 11: 300-11.
23. Ouyang ML, Xia HW, Xu MM et al. Prediction of occult lymph node metastasis using SUV, volumetric parameters and intratumoral heterogeneity of the primary tumor in T1-2N0M0 lung cancer patients staged by PET/CT. *Ann Nucl Med* 2019; 33: 671-80.
24. Kim DH, Song BI, Hong CM et al. Metabolic parameters using ^{18}F-FDG PET/CT correlate with occult lymph node metastasis in squamous cell lung carcinoma. *Eur J Nucl Med Mol Imaging* 2014; 41: 2051-7.
25. Pieterman RM, van Putten JW, Meuzelaar JJ et al. Preoperative staging of non-small-cell lung cancer with positron-emission tomography. *N Engl J Med* 2000; 343: 254-61.

26. Cong M, Yao H, Liu H et al. Development and evaluation of a venous computed tomography radiomics model to predict lymph node metastasis from non-small cell lung cancer. *Medicine (Baltimore)* 2020; 99: e20074.
27. Huang Y, Jiang X, Xu H et al. Preoperative prediction of mediastinal lymph node metastasis in non-small cell lung cancer based on ^{18}F-FDG PET/CT radiomics. *Clin Radiol* 2023; 78: 8-17.
28. Dai M, Wang N, Zhao X et al. Value of Presurgical ^{18}F-FDG PET/CT Radiomics for Predicting Mediastinal Lymph Node Metastasis in Patients with Lung Adenocarcinoma. *Cancer Biother Radiopharm* 2024; 39: 600-10.
29. Chang C, Ruan M, Lei B et al. Development of a PET/CT molecular radiomics-clinical model to predict thoracic lymph node metastasis of invasive lung adenocarcinoma ≤3 cm in diameter. *EJNMMI Res* 2022; 12: 23.
30. Ouyang ML, Wang YR, Deng QS et al. Development and Validation of a ^{18}F-FDG PET-Based Radiomic Model for Evaluating Hypermetabolic Mediastinal-Hilar Lymph Nodes in Non-Small-Cell Lung Cancer. *Front Oncol* 2021; 11: 710909.
31. Zhang R, Zhang R, Luan T et al. A Radiomics Nomogram for Preoperative Prediction of Clinical Occult Lymph Node Metastasis in cT1-2N0M0 Solid Lung Adenocarcinoma. *Cancer Manag Res* 2021; 13: 8157-67.
32. Zhong Y, Yuan M, Zhang T et al. Radiomics Approach to Prediction of Occult Mediastinal Lymph Node Metastasis of Lung Adenocarcinoma. *Am J Roentgenol* 2018; 211: 109-13.
33. Qiao J, Zhang X, Du M et al. ^{18}F-FDG PET/CT radiomics nomogram for predicting occult lymph node metastasis of non-small cell lung cancer. *Front Oncol* 2022; 12: 974934.
34. Wang L, Li T, Hong J et al. ^{18}F-FDG PET-based radiomics model for predicting occult lymph node metastasis in clinical N0 solid lung adenocarcinoma. *Quant Imaging Med Surg* 2021; 11: 215-25.
35. Yang X, Pan X, Liu H et al. A new approach to predict lymph node metastasis in solid lung adenocarcinoma: a radiomics nomogram. *J Thorac Dis* 2018; 10: S807-S819.